Seasonal Cross-Shelf Flow Structure, Upwelling Relaxation, and the Alongshelf Pressure Gradient in the Northern California Current System*

RYAN M. MCCABE

Joint Institute for the Study of the Atmosphere and Ocean, University of Washington, Seattle, Washington

BARBARA M. HICKEY

School of Oceanography, University of Washington, Seattle, Washington

EDWARD P. DEVER

College of Earth, Ocean, and Atmospheric Sciences, Oregon State University, Corvallis, Oregon

PARKER MACCREADY

School of Oceanography, University of Washington, Seattle, Washington

(Manuscript received 7 February 2014, in final form 15 October 2014)

ABSTRACT

Moored observations are used to investigate the seasonal change in vertical structure of the cross-shelf circulation at a midshelf location in the northern California Current System. A streamwise–normal coordinate system is employed to eliminate meander- and eddy-induced biases in the cross-shelf flow that are unaccounted for with an alternative, commonly applied approach. The resulting flow structure develops an organized pattern midway through the upwelling season. In particular, under upwelling-favorable conditions an onshore return layer occurs just beneath the offshore surface flow, and a third offshore-directed layer exists at depth that does not appear to satisfy Ekman dynamics (to within 9 m of the bottom). Both subsurface layers strengthen in time over the upwelling season. Mechanisms to explain the mean structure are evaluated, and it is suggested that the timing of the development and strengthening of both the interior onshore return flow and the offshore near-bottom layer are consistent with the seasonally changing direction and magnitude of the large-scale alongshelf sea level gradient. The change to a poleward sea level gradient initiates a seasonal relaxation of upwelled isopycnals that likely leads to the near-bottom flow. Late-season enhancement of the interior onshore return flow is related to the alongshelf surface wind stress but appears to form as a consequence of offshore transport in the near-bottom layer and the need to satisfy coastal mass balance.

1. Introduction

Cross-shelf exchange is one of the most important, but least understood, physical phenomena in the coastal ocean. Exchange processes regulate heat and salt distributions (Lentz 1987; Rudnick and Davis 1988; Dever and Lentz 1994; Weingartner et al. 2005), nutrient availability (Jacox and Edwards 2011), and dissolved oxygen concentrations (Wiseman et al. 1997; Rabalais et al. 2002). Similarly, larval recruitment (Johnson et al. 1986; Roughgarden et al. 1988; Blanton et al. 1995; Wing et al. 1995) and plankton transport (MacFadyen et al. 2005) are impacted by the same physical mechanisms that force exchange.

Because it is central to the upwelling problem, many previous studies have investigated cross-shelf exchange in eastern boundary current (EBC) systems. Comparisons of results from early observational efforts off the coast of Oregon (OR), Peru, and northwest Africa are provided by Smith (1981) and Allen and Smith (1981). Although Ekman dynamics appear to hold in the surface

* Pacific Northwest Toxins Contribution Number 12, Ecology and Oceanography of Harmful Algal Blooms Contribution Number ECO809, and Joint Institute for the Study of the Atmosphere and Ocean Contribution Number 2383.

Corresponding author address: Ryan M. McCabe, University of Washington, Joint Institute for the Study of the Atmosphere and Ocean, Box 355672, 3737 Brooklyn Ave. NE, Seattle, WA 98195.
E-mail: rmccabe@ocean.washington.edu

DOI: 10.1175/JPO-D-14-0025.1

layer (Smith 1981; Winant et al. 1987; Lentz 1992; Dever 1997b), the dynamics of subsurface cross-shelf transports are less clear, particularly since the subsurface response varies significantly across systems (Smith 1981). The lack of understanding stems in part from cross-shelf exchange being difficult to accurately isolate; cross-shelf flows are generally much weaker than coincident alongshelf flows, they have short correlation length scales (<20 km; Kundu and Allen 1976; Dever 1997a), and water column velocity measurements often do not span the crucial surface and bottom boundary layers.

To help address the varying responses among shelf systems described by Smith (1981), Lentz and Chapman (2004) presented a theory relating the vertical structure of onshore upwelling ''return'' flows to stratification (quantified with the buoyancy frequency N), the bottom slope α, and latitude (through the Coriolis parameter f) via steady nonlinear momentum dynamics. They show that when the ratio $\alpha N/f$ is relatively large ($\sim$1 or greater), return flows tend to be shallower in the water column, and there is a greater contribution from nonlinear momentum fluxes; when $\alpha N/f$ is relatively small ($\sim$0.5 or less), nonlinear terms are small relative to the wind stress, and onshore return flows are concentrated near the bottom. Although the Lentz and Chapman (2004) theory also included the effects of a mean alongshelf pressure gradient, its impacts were not explored in detail since variations in $\alpha N/f$ accounted for much of the observed variability in the vertical structure of cross-shelf exchange in their model.

Because alongshelf pressure gradients are fundamental forcing components in EBC systems, it is likely that some aspect of the structure and variability of cross-shelf exchange will depend on them. In the California Current System (CCS; Kundu and Allen 1976; Allen and Kundu 1978; Battisti and Hickey 1984; Chapman 1987) and the Humboldt Current System off the coast of Peru (Smith 1978; Brink et al. 1980), remotely forced pressure perturbations in the form of propagating coastal-trapped waves (CTWs) represent the leading source of variability in alongshelf flows ($\sim$90% off the coast of OR; Kundu et al. 1975). However, CTW theory has historically failed at predicting variability in observed cross-shelf flows (Chapman 1987), and the addition of CTW variability to numerical models has not improved model data cross-shelf velocity comparisons (Zamudio and Lopez 1994). It is possible that such discrepancies stem from the aforementioned difficulty in isolating the relatively weak cross-shelf circulation from time series observations.

Large-scale mean alongshelf pressure gradients (APGs) also force circulation in the coastal ocean (e.g., Bryden 1978). The existence of a mean sea level slope $O(10^{-7})$ was first suggested by Stommel and Leetmaa (1972) as a way to explain circulation in the Middle Atlantic Bight off the eastern United States. Off the coast of Western Australia, a particularly large mean APG overcomes equatorward wind stress to force the Leeuwin Current poleward [Thompson 1987; Smith et al. 1991; also see the recent analysis of Rossi et al. (2013)]. Huyer et al. (1987) presented data suggesting that upwelling off the coast of Peru in 1983 was inhibited by a large mean APG. When Federiuk and Allen (1995) imposed a mean APG in their upwelling model, they noted improvement in alongshelf velocity statistics and a reduction in the near-bottom cross-shelf flow that was closer to observations. More recently, Marchesiello et al. (2010) argue that a mean APG could explain the limited upwelling off the coast of northern New Caledonia, while Marchesiello and Estrade (2010) show that a revised upwelling index that includes APG-forced cross-shelf geostrophic flows agrees better with an SST-based index in each of the four major upwelling systems.

In the northern CCS, the region of interest in our present study, Hickey and Pola (1983) used observations to demonstrate a seasonally reversing APG. They employed the arrested wave dynamics of Csanady (1978) to show that the APG results from the alongshelf distribution of alongshelf wind stress throughout the CCS. Subsequent numerical experiments, including both wind stress and mean APG forcing, suggest that the reversing APG is important in driving seasonal-mean alongshelf and cross-shelf flows including undercurrents (Werner and Hickey 1983). Although mean APGs are fundamental components in EBC systems, observational evidence for them, and for their impact on cross-shelf exchange, remains scarce.

Upwelling ''relaxation'' is another process that impacts coastal exchange. Relaxation events happen when upwelling-favorable wind stress weakens and isopycnals that are tilted up toward the coast fall back toward a flat state. This process is associated with shoreward advection of near-surface water and has been shown to control larval recruitment (Farrell et al. 1991). Idealized simulations by Hamilton and Rattray (1978) showed near-surface isopycnals retreating toward shore after upwelling winds ceased, while the alongshelf velocity decreased on a time-scale similar to that of upwelling spinup (i.e., a few days). Austin and Barth (2002) empirically fit an exponential curve to observations of a particular isopycnal in order to model wind-induced variability of the upwelling front off the coast of OR. They found that after upwelling events, isopycnals tended to relax shoreward toward geostrophic equilibrium on a time scale of roughly 8 days, consistent with the picture provided by Hamilton and Rattray (1978).

Off the coast of northern California (CA), weakening upwelling-favorable winds also give rise to nearshore, poleward, alongshelf flows (Kosro 1987; Send et al. 1987). Explanations for the poleward flows involve interaction of the alongshelf jet with rough topography (Send et al. 1987; Gan and Allen 2002) and alongshelf changes in shelf width and wind forcing (Pringle and Dever 2009) that give rise to alongshelf differences in upwelled water properties. In both scenarios, APGs are set up that force the relaxation flows. Similar responses have been documented off the coast of central CA (Ramp et al. 2005; Melton et al. 2009) and the Iberian Peninsula (Relvas and Barton 2002, 2005). In spite of these various studies, and the relatively well understood seasonality in our own region (Huyer et al. 1975, 1978; Freeland et al. 1984; Strub et al. 1987; Hickey 1989), no clear picture of the longer-term seasonal relaxation of an upwelling jet has been described.

In this manuscript, we present observations of cross-shelf circulation from a 2005 midshelf site in the northern CCS that show influences of both fluctuating and mean alongshelf pressure gradients. We begin with a brief description of the data sources used in this study (section 2) before examining the core time series in section 3. Two different techniques for extracting a two-dimensional (2D) representation of the cross-shelf circulation are presented and compared: a commonly used method and a new approach aimed at avoiding meander- or eddy-induced biases in the final structure. Results show time-variable cross-shelf flow patterns in early summer but a more stable pattern later in the season where, under upwelling-favorable conditions, offshore surface transport is observed, with onshore return flow at middepth and offshore flow beneath. Monthly averaged upwelling-favorable circulation profiles are examined in section 4, and potential mechanisms to explain the observed exchange are evaluated in section 5. We suggest that a mean alongshelf pressure gradient likely leads to the observed flow structure. After a brief discussion in section 6, the paper concludes with a summary of our findings (section 7).

2. Data sources

Primary data presented in this paper were collected in 2005 as part of the River Influences on Shelf Ecosystems (RISE) program, an interdisciplinary project aimed at understanding biological impacts of the Columbia River plume (Hickey et al. 2010). RISE mooring placement was designed to contrast conditions near the river mouth with those farther north and south on the Washington (WA) and OR shelves. Specifically, a centrally located mooring was placed off the Columbia River mouth, a southern mooring was placed on the OR midshelf, and a northern mooring RN was placed on the WA midshelf (72-m isobath). Of the two moorings positioned away from the Columbia River, RN captured the highest percentage of the water column (83% compared to 69% at the OR site). For this reason, data from the RN mooring are the focus of this paper; its location is shown in Fig. 1.

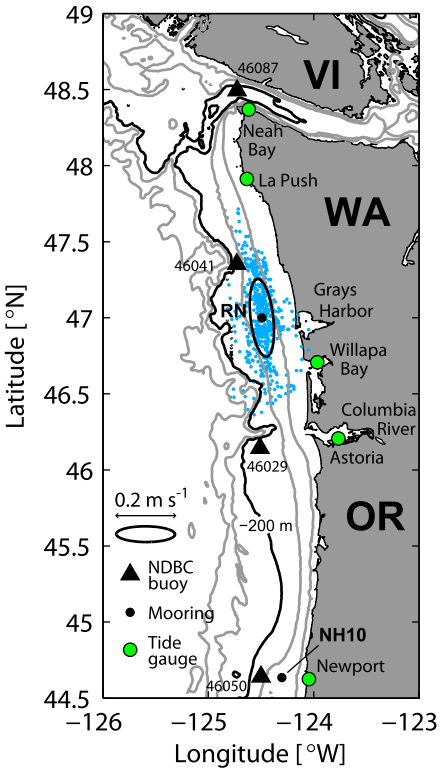

FIG. 1. Map of the northern CCS showing the location of the midshelf RN mooring off Grays Harbor, WA, in 2005 (black circle; 72-m bottom depth), the NH10 mooring off Newport, OR (black circle; 81-m bottom depth), coastal NDBC buoys (black triangles), and available tide gauges (green circles). Blue dots represent dispersion of the depth-averaged subtidal currents at RN (only data every 6 h are plotted); the black ellipse represents the principal axes of variation of those currents (the major axis is oriented approximately 10° counterclockwise of true north). The shelf break, denoted by the −200-m isobath, is black. Other bathymetry contours (−50, −100, −500, and −1000 m) are gray.

Water column velocity measurements at RN were made with a downward-looking 300-kHz acoustic Doppler current profiler (ADCP) mounted on a surface buoy (as in Dever et al. 2006). In such configurations, surface wave–induced vertical motion of the instrument may bias velocity records (Pollard 1973). An analysis of such errors made using surface wave data from a nearby (24.5 km) wave buoy off Grays Harbor, WA, showed a <10% change in the surface 15-m layer-averaged cross-shelf velocities when the wave bias was removed; this effect did not significantly alter the velocity structures

presented herein. Velocity ensembles were recorded at 7.5-min intervals in 0.5-m bins. These data were processed using standard techniques and averaged to hourly intervals in 2-m bins. The processed record spans the water column from 3- to 63-m depth [or 9 m above bottom (mab)]. The hourly velocity data were low-pass filtered using a cosine–Lanczos window (40-h half amplitude, 46-h half power; see, e.g., Beardsley et al. 1985) in order to examine subtidal variability. A dispersion diagram of the depth-averaged subtidal currents is included in Fig. 1 (blue dots); the black ellipse represents the principal axes of variation of those currents. Velocity data were rotated into a coordinate frame aligned with the axes of this ellipse. Because the ellipse major axis reasonably approximates the direction of local isobaths (to within ~5°), we refer to the rotated coordinates as alongshelf (y; positive north) and cross-shelf (x; positive onshore), respectively.

Water property data from RN and supporting water property and velocity data from a U.S. Global Ocean Ecosystems Dynamics (GLOBEC) northeast Pacific shelf mooring (the NH10 mooring on the 81-m isobath off Newport, OR; Fig. 1) were also averaged to hourly values and then low-pass filtered with the same filter used for the RN velocity data. NH10 data were subsequently decimated to 6-h intervals.

In addition, several hundred conductivity–temperature–depth (CTD) profiles were made off WA as part of both the RISE and Ecology and Oceanography of Harmful Algal Blooms–Pacific Northwest (ECOHAB–PNW; MacFadyen et al. 2008) projects. Each project conducted two cruises in 2005 that sampled with Sea-Bird Electronics 911plus systems. Hydrographic data were processed into 1-m bins using standard Sea-Bird software. Quality control included using primary and secondary sensors, pre- and postcruise calibrations, and salinity regressions with bottle samples.

Other data sources include meteorological observations from various National Data Buoy Center (NDBC) coastal buoys and sea level from coastal tide gauges (see Fig. 1 for locations in the region). Hourly records of wind speed and direction were used to form estimates of surface stress (Large and Pond 1981), which were also low-pass filtered using the same filter applied to the water column velocity data. Hourly sea level data were obtained from the National Oceanic and Atmospheric Administration (NOAA) National Ocean Service (NOS) online archive and the University of Hawaii Joint Archive for Sea Level. These data were corrected for the inverse barometer effect (forming adjusted sea level) by adding hourly records of atmospheric pressure converted to a sea level equivalent at each station (e.g., Gill 1982). In most cases, linear regressions with other nearby atmospheric pressure records were necessary to complete the atmospheric pressure record for any given site ($R^2 \geq 0.87$ in all instances).

3. Time series observations

a. Overview and basic patterns

Key subtidal time series of forcing including alongshelf wind stress τ^y and sea level slope η_y and the alongshelf and cross-shelf current response (v and generally u, respectively) are presented in Fig. 2. Alongshelf current variability on 3–10-day time scales is evident (Fig. 2c), typical of local (Fig. 2a) and remote (Fig. 2b) wind forcing in the region (Hickey 1984, 1989). June and the first half of July experienced variable winds with frequent reversals (Fig. 2a). Although the "spring transition" to upwelling-favorable conditions occurred on 24 May (Kosro et al. 2006), persistently equatorward τ^y did not occur off WA until mid-July. After this time, the relatively strong equatorward τ^y is clearly associated with equatorward v (Fig. 2c). This pattern persists until τ^y weakens in late August and north–south v reversals, associated with η_y fluctuations (Figs. 2b,c), dominate the alongshelf response.

The two measures of cross-shelf circulation (Figs. 2d,e; discussed in more detail in section 3b) appear similar and show some expected, and some unexpected, results. In particular, offshore surface flows tend to be associated with equatorward τ^y events, consistent with Ekman dynamics. At times of poleward v (Fig. 2c), the corresponding u flows resemble the expected downwelling-favorable circulation, with onshore flow near the surface and offshore flow at depth (Figs. 2d,e). However, under upwelling-favorable conditions, the subsurface cross-shelf flow response changes dramatically with season. Early in the record the cross-shelf circulation is quite variable; at times, onshore return flows occur in the middle, or "interior," of the water column, whereas other events have return flows concentrated in the lower water column (hereafter referred to as near bottom). Beginning in approximately late July or early August, a consistent pattern emerges: a concentrated onshore return flow exists in the interior with a primarily offshore-directed flow beneath (Figs. 2d,e).

Differences between the two measures of cross-shelf circulation are plotted in Fig. 2f and are discussed further below. The final panel (Fig. 2g) presents a time series of the direction of the depth-averaged subtidal flow relative to the equatorward alongshelf direction (0°), further illustrating that shelf flows at RN were quite variable and often veered toward or away from shore. For example, during the relatively quiescent upwelling-favorable period from 15 July to 25 August, the direction of the depth-averaged current has a standard deviation

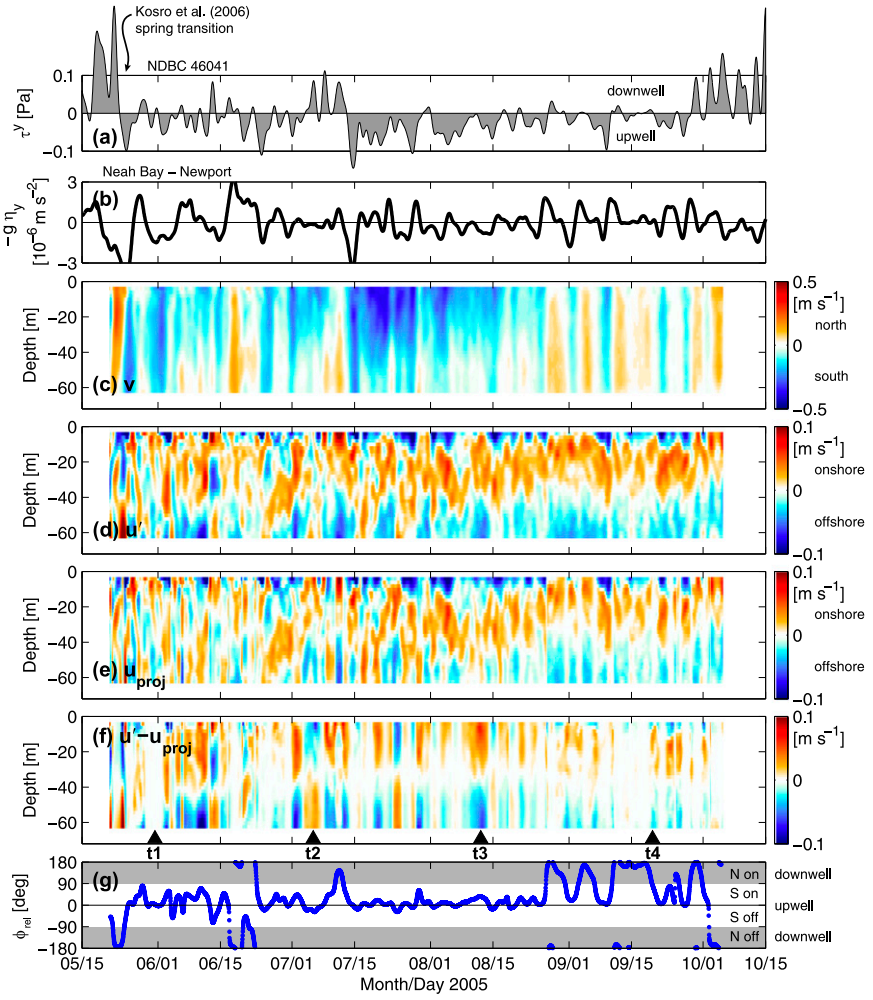

FIG. 2. Time series observations including (a) low-pass filtered alongshelf surface wind stress from NDBC buoy 46041 (positive poleward or downwelling favorable), (b) the subtidal surface pressure gradient calculated by differencing demeaned tide gauge observations from Neah Bay, WA, and Newport, OR, and (c) observed subtidal alongshelf currents (positive poleward or north; downwelling favorable) from the midshelf RN mooring (see Fig. 1 for location). (d),(e) Two different measures of the cross-shelf circulation (positive onshore) are shown and are discussed in section 3b; (f) their difference is shown. Black triangles at the bottom of (f) indicate four different times (t1–t4) referred to in Fig. 4. (g) The direction of the depth-averaged subtidal flow relative to the southward alongshelf direction (0°). Gray shading indicates a downwelling-favorable [poleward or northward (N)] flow; upwelling-favorable [equatorward or southward (S)] flows are contained within the white band. For reference, these conditions are labeled at the right, as are whether the depth-averaged flow has an on- or off-shelf component.

of 15°. For a typical alongshelf flow $O(10)\,\mathrm{cm\,s^{-1}}$, this degree of veering would give rise to an apparent cross-shelf flow $O(2.6)\,\mathrm{cm\,s^{-1}}$, which is reasonably large in comparison to typical cross-shelf velocities.

b. Isolating the cross-shelf circulation

1) THE TRADITIONAL APPROACH: u'

Cross-shelf flows are typically weak compared to coincident alongshelf currents, and mean flow variability often results in unbalanced momentum (Allen and Smith 1981). For this reason, the instantaneous depth-averaged cross-shelf flow is usually removed from the measured cross-shelf velocity record:

$$u' = u - \overline{u}, \tag{1}$$

(e.g., Dever 1997b; Lentz 2001), where u is the measured cross-shelf velocity component and $\overline{u} = H^{-1}\int_{-H}^{0} u\,dz$,

where H is the depth, and z is the vertical coordinate. This approach forces 2D mass balance, making analysis and dynamical interpretation of the results tractable. Since velocity observations rarely cover the entire water column, in some studies the velocity profiles are uniformly extended to the surface and bottom boundaries from the shallowest and deepest measurements, respectively, before calculating the depth-averaged flow (Lentz 2001; Lentz and Chapman 2004). Doing this did not substantially change our own results, so instead we calculate u' (Fig. 2d) using only the directly measured profile (i.e., 3–63-m depth or to 9 mab).

However, if the alongshelf flow is vertically sheared (Fig. 2c) and veers over slightly to cross the local isobaths (Fig. 2g), removal of the depth-averaged cross-shelf flow can leave biases in the resulting u' signal, as will be illustrated in section 3b(3). To avoid such meander- or eddy-induced biases but retain a 2D balance, we instead use an alternative approach, which is described next.

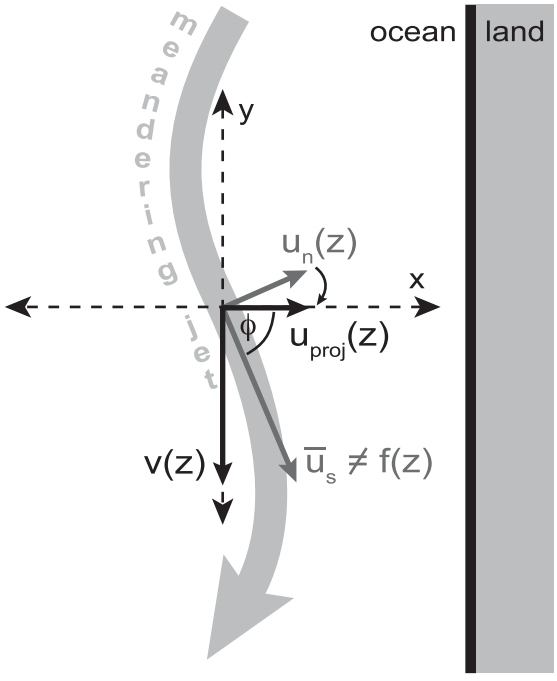

FIG. 3. Plan view schematic illustrating the calculation of u_{proj} when the alongshelf current has veered toward shore. The streamwise direction is aligned with the depth-averaged current $\overline{u}_s$, which is at an angle ϕ relative to the cross-shelf coordinate x. The depth-dependent stream-normal circulation u_n is calculated relative to the $\overline{u}_s$ direction, and by definition depth integrates to zero. The component of u_n in the cross-shelf direction is given by u_{proj}.

2) AN ALTERNATIVE APPROACH: u_{proj}

A streamwise–normal ($s - n$) coordinate system,

$$s = x\cos\phi + y\sin\phi, \tag{2}$$

$$n = y\cos\phi - x\sin\phi, \tag{3}$$

is adopted where the along-stream coordinate s is aligned with the strongest signal, the direction of the instantaneous depth-averaged velocity $\overline{u}_s$ (Fig. 3; Rozovskii 1957; Kalkwijk and Booij 1986; Geyer 1993). The stream-normal velocity u_n is then extracted relative to this along-stream direction and by definition depth integrates to zero. In (2) and (3), ϕ is the angle of the depth-averaged streamwise flow relative to the $x - y$ system. Primary assumptions in this calculation are that the depth-averaged flow is well sampled and that it serves as a meaningful indicator of actual motion on the shelf. If, for example, the alongshelf flow were composed of two layers with equal transports flowing in opposite directions, then this approach would be less useful. Because shelf flows are nominally oriented parallel to local isobaths, and the coastal waveguide is along the shelf, it is important to quantify the portion of the flow actually crossing the isobaths. This is achieved by a simple geometric projection of the stream-normal component u_n onto the cross-shelf coordinate (Fig. 3) forming u_{proj}, an estimate of the cross-shelf velocity less any influences resulting from mean flows such as veering of the alongshelf current (Fig. 2e). Alongshelf current veering still may provide large episodic cross-shelf transports, but our present focus is on the residual component relative to the veering since we expect it to be better related to identifiable forcing agents and therefore more predictable.

3) COMPARING u' AND u_{proj}

Although the independent series of u' (Fig. 2d) and u_{proj} (Fig. 2e) appear quite similar, their difference $u' - u_{proj}$ (Fig. 2f) is not small relative to either u' or u_{proj}. Instantaneous profiles of u' and u_{proj}, their difference $u' - u_{proj}$, and the speed of the flow in the depth-averaged flow direction at four selected times, are shown in Fig. 4. The timing for each row of Fig. 4 is indicated by the four black triangles at the bottom of Fig. 2f. First consider the top row of panels in Fig. 4a. At this time ($t1$, just before 1 June) the u' and u_{proj} profiles are nearly identical. During the second event ($t2$; Fig. 4b), u' is noisy with no clear circulation pattern, whereas u_{proj} indicates that a two-layer downwelling-favorable cross-shelf flow exists. Their difference (middle column, Fig. 4b) is upwelling-favorable at a time when the depth-averaged flow is directed offshore (Fig. 2f). The difference profile is

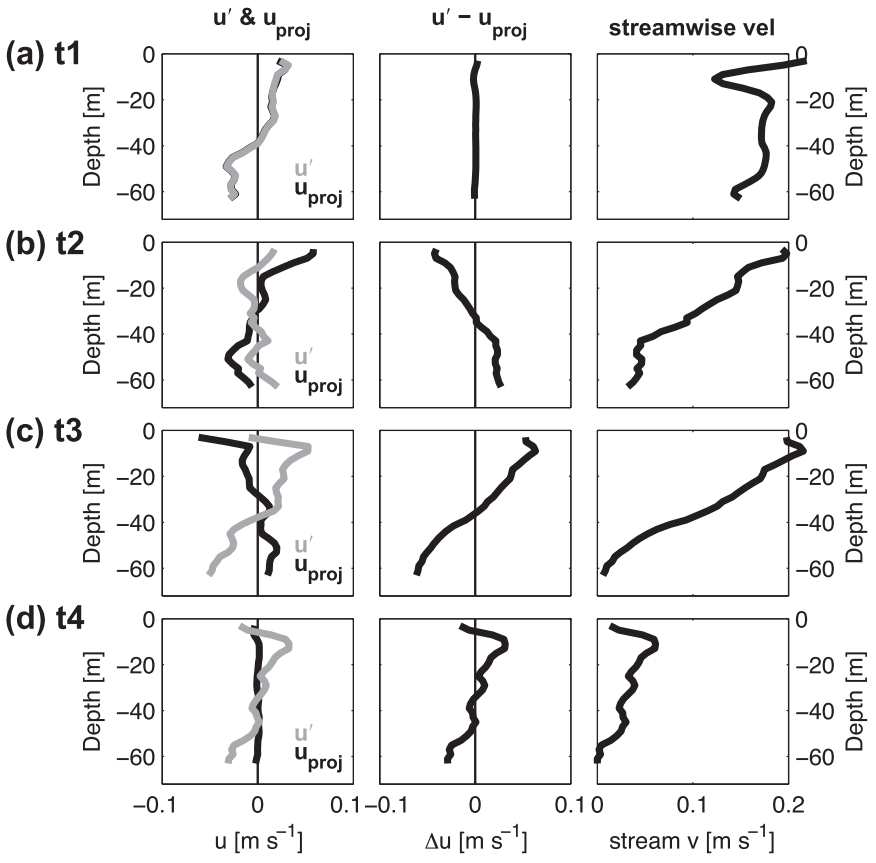

FIG. 4. Instantaneous profiles of (left) u' and u_{proj}, (middle) their difference $u' - u_{\text{proj}}$, and (right) the speed of the flow in the depth-averaged direction. The timing for each row ($t1$–$t4$) is indicated by the four black triangles at the bottom of Fig. 2f.

simply a fraction of the streamwise flow profile shown in the rightmost column (with its depth-averaged value removed). At time $t3$ (Fig. 4c), u' and u_{proj} give opposite cross-shelf velocity profiles; u' indicates a largely downwelling-favorable signal that appears to be overwhelming offshore surface Ekman transport, while u_{proj} presents an upwelling-favorable flow profile. Referring to Fig. 2g, we see that the depth-averaged flow direction at this time has an onshore component, and again the difference profile resembles the streamwise flow. The final event ($t4$; Fig. 4d) shows that the u' signal is nothing more than the streamwise velocity profile with its depth-averaged value removed.

In summary, our results demonstrate that u' is biased by the streamwise velocity profile and that this bias is enough to overwhelm the cross-shelf velocity signal as quantified by u_{proj}. For the current dataset, we believe u_{proj} represents the best estimate of the "uncontaminated" 2D cross-shelf flow. For the remainder of this paper, we focus on the seasonal evolution of the cross-shelf circulation under upwelling-favorable conditions.

4. Seasonal-mean velocity structure during upwelling-favorable conditions

To gain insight into the seasonally changing vertical structure during active coastal upwelling, we next examine monthly averaged quantities. Mean alongshelf and cross-shelf velocity profiles from the RN mooring were averaged over each of the four months of June–September 2005 (Fig. 5), but only for times when both the wind stress and the depth-averaged alongshelf flow were equatorward (both upwelling favorable). The number of days in a given month meeting these criteria is written in the left-side panels next to the v profiles. We chose to average over upwelling events because downwelling-favorable or poleward flow events have a stable, approximately two-layered cross-shelf velocity profile with strong offshore-directed flows at depth (Fig. 2). Omitting downwelling-favorable conditions should better isolate the true upwelling velocity structure.

Mean alongshelf currents vary considerably in both magnitude and vertical shear throughout the upwelling

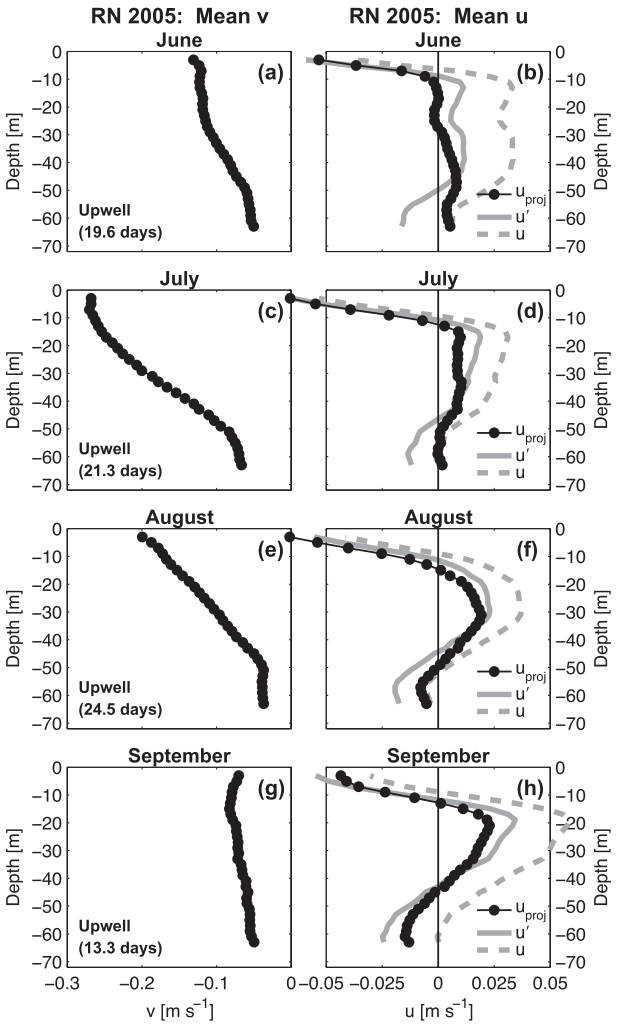

FIG. 5. Mean upwelling velocity profiles from the 2005 RN midshelf mooring off the coast of WA. Averages are computed during upwelling conditions in the months of (top to bottom) June, July, August, and September. The number of days used in the mean is written in text in the left-side panels. (left) Mean alongshelf velocity v (negative southward). (right) Three estimates of the mean cross-shelf velocity (negative offshore): u the measured subtidal signal (dashed gray line), u' the measured signal with the depth-averaged value removed (solid gray line), and u_{proj} (black dots).

season (Fig. 5, left-side panels). Average vertical shear peaks in July and then decreases throughout the remainder of the record. Substantial differences in the corresponding mean cross-shelf currents also exist (Fig. 5, right-side panels). Each month exhibits a mean offshore surface-trapped flow consistent with surface Ekman dynamics, but the structure of the subsurface profiles changes as the upwelling season progresses. Specifically, the onshore return flow, as quantified by u_{proj}, appears deep in the water column in June (Fig. 5b), but concentrated in the interior (between ~15- and 45-m depth) from July to September (Figs. 5d,f,h). The depth of this return flow maximum shoals over time, and its peak magnitude more than doubles from early to late season. Mean near-bottom cross-shelf currents (below ~50-m depth) also change dramatically, from weak and onshore in June, to near zero in July, and then become increasingly offshore in August and September; the strongest near-bottom offshore flows coincide with the strongest onshore interior return flows. What causes this seasonal change in structure? In the following section, we examine different possible mechanisms that could help explain the changes in the mean cross-shelf velocity profile.

5. Possible mechanisms responsible for the evolving mean structure of the cross-shelf circulation

a. *Alongshelf wind stress*

Alongshelf wind stress is thought to be the primary mechanism driving cross-shelf exchange in upwelling systems. Surface layer transport calculations, using extended versions of the mean profiles in Fig. 5 (i.e., uniformly to the surface and bottom) summed to the first zero crossing beneath the surface, were all within 25% of theoretical transports derived using mean τ^y estimates ($0.3–0.45\,\text{m}^2\,\text{s}^{-1}$, with layer-averaged velocities in the $2.5–4.1\,\text{cm}\,\text{s}^{-1}$ range), consistent with Ekman dynamics. Prior observations in the northern CCS have shown significant onshore return flows within the interior water column (Bryden 1978; Smith 1981; Hickey 1989). In the present case, τ^y decreases after July (Fig. 2a), whereas the onshore interior flow increases (Fig. 5). By September the upwelling-averaged interior transport exceeds that in the surface layer by ~75% (Fig. 5). This suggests that direct forcing by the alongshelf wind stress itself cannot fully account for the seasonal pattern of the observed return flow.

b. *Changes in stratification*

As discussed in section 1, Lentz and Chapman (2004) relate the vertical structure of the mean cross-shelf circulation to the ratio $\alpha N/f$, showing that onshore return flows tend to be concentrated higher in the water column when $\alpha N/f$ is larger (~1 or greater). At a set location such as the RN mooring site, only N changes in time. To examine the seasonal progression of water column stratification, monthly averaged profiles of N^2 are plotted in Fig. 6. The profiles were averaged from shipboard CTD casts taken during four cruises over the WA midshelf ($50\,\text{m} \le z_{\text{bot}} \le 100\,\text{m}$; with z_{bot} the bottom depth) in 2005. Mean stratification decreases over the course of the upwelling season, with interior N smaller by a factor of approximately 1.7 in September compared to June (Fig. 6). Since the shallowest return flows occur late in

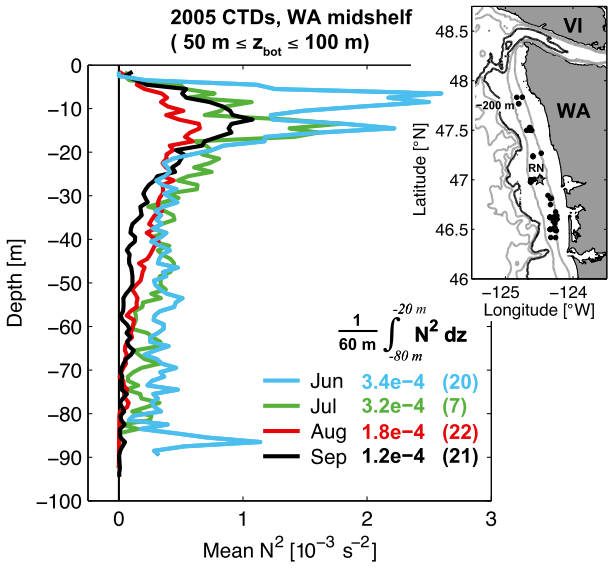

FIG. 6. Monthly-mean N^2 profiles from shipboard CTD casts made over the WA midshelf (50 m ≤ z_{bot} ≤ 100 m) in 2005. Vertically averaged mean values spanning the interior 60 m of the water column (20–80-m depths) are displayed in the text at the lower right. The number of casts used to compute the mean profiles for each month is given in parentheses. Cast locations are shown in the inset where bathymetry contours are drawn at −50, −100, −200, −500, and −1000 m (where the −200-m contour is drawn black). For reference, the RN mooring location (gray star) is also labeled. Mean midwater N decreases by a factor of ~1.7 from June to September.

the season when N has decreased (August–September; Fig. 5), it appears that changes in N alone are not sufficient to explain the seasonally changing structure of cross-shelf circulation over the WA midshelf.

As a consistency check, we also calculated the nonlinear cross-shelf momentum flux divergence assuming a zero flux/zero velocity condition at the coast (Lentz and Chapman 2004). This nonlinear term was insignificant relative to the alongshelf wind stress term in the depth-integrated momentum equation, and monthly averaged depth profiles of $u_{proj}v_x$ (averaged during the same time periods in Fig. 5) were an order of magnitude less than the Coriolis force associated with the cross-shelf flow (not shown). Although these estimates of the nonlinear term should be taken with caution, the results are consistent with Fig. 6 and our above conclusion and suggest that other dynamics are active.

c. Bottom stress and the near-bottom flow

The RN velocity record only extended to 9 mab, and the late-season mean currents at that depth are inconsistent with bottom Ekman dynamics (Fig. 5). To test for near-bottom frictional influences, we examined profiles of current directions with depth above the 9-m cutoff (not shown). This analysis revealed distinct counterclockwise rotation with depth during poleward flows, but only intermittent rotation with depth during equatorward flows, consistent with thicker frictional layers during downwelling-favorable events (Lentz and Trowbridge 1991). The lack of persistent rotation during equatorward flows suggests that the observations at 9 mab were often near the top of a frictional layer during upwelling; at times friction may influence the flow in the observed near-bottom layer, while at other times it may not. It is unknown whether the alongshelf or cross-shelf flows may reverse closer to the bottom. Lacking additional data beneath the deepest observations, we are unable to accurately determine the role of bottom stress in forcing the observed near-bottom cross-shelf flow. Since both the nonlinear term (section 5b) and tendency term are of insufficient magnitude ($<10^{-7}$ m s^{-2}) to balance the Coriolis force associated with the near-bottom offshore flow, we assume this flow must result from either bottom stress or as a residual of the other terms in the alongshelf momentum equation.

d. Alongshelf pressure gradient

In the northern CCS, CTWs are ubiquitous (e.g., Kundu et al. 1975; Battisti and Hickey 1984; Hickey 1984), and a large-scale mean surface APG is well documented (Hickey and Pola 1983). Potential contributions from each of these factors to the mean cross-shelf velocity profiles are discussed next.

1) CONTRIBUTIONS FROM FLUCTUATING ALONGSHELF PRESSURE GRADIENTS

In the northern CCS, the fluctuating component of the alongshelf pressure gradient (associated with CTW activity) is a significant part of the depth-averaged alongshelf acceleration (Hickey 1984). Calculations using linear inviscid dynamics,

$$v_t + fu_{CTW} = -\rho_0^{-1}P_y, \tag{4}$$

(e.g., Chapman 1987) with the alongshelf velocity (Fig. 2c) and adjusted coastal sea level data (Fig. 2b) indicate that u_{CTW}, the interior cross-shelf flow resulting from a passing CTW, is reasonably small (≤1 cm s^{-1}) and nearly vertically uniform (not shown). If we consider only CTW forcing, then the Fig. 5 profiles would have been averaged over the "upwelling phase" of a passing wave (the portion of the wave with equatorward alongshelf flow). Although bottom stress acting on the equatorward alongshelf flow should force near-bottom onshore transport, the interior cross-shelf velocity u_{CTW} during the upwelling-phase of a first-mode CTW may be offshore. To test whether or not CTW

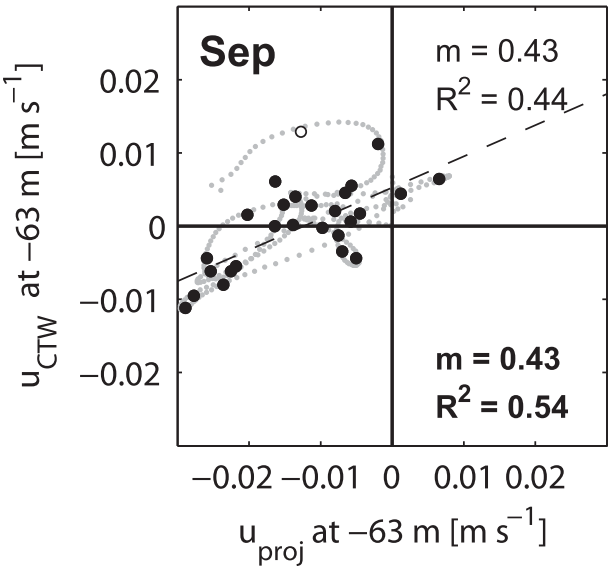

FIG. 7. Scatter diagram of u_{proj} vs u_{CTW} during upwelling-favorable time periods in September 2005, the only month with a significant relationship. Small gray dots are the individual hourly (but subtidal) data points. Black dots represent the independent observations, estimated as integral time-scale averages of the subtidal hourly data (one point per effective degree of freedom). A least squares fit to the black dots is drawn as the dashed line. Slopes (m) and R^2 values for the fit are shown for all black dots (normal font, upper right) and for the case with the open circle omitted (bold font, lower right).

dynamics can account for the mean near-bottom offshore transport in Figs. 5f and 5h, potentially as a result of CTW phase aliasing in our upwelling-only averages, we plotted observed u_{proj} from the bottommost ADCP bin against u_{CTW} predicted using (4) for the same time periods considered in Fig. 5. September was the only month with a significant relationship (Fig. 7), consistent with the timing of the alongshelf flow reversals seen in Fig. 2c. Nevertheless, variability of u_{CTW} was, on average, only half as large as observed, and more importantly u_{CTW} had a near-zero mean (Fig. 7). We conclude that while CTW dynamics likely influence event-scale variability of the observed cross-shelf circulation, for the present dataset they do not convincingly account for the observed late-season mean near-bottom offshore flow.

2) THE CONTRIBUTION FROM A LARGE-SCALE MEAN ALONGSHELF SEA LEVEL GRADIENT

Hickey and Pola (1983) document a seasonal reversal of the mean alongshelf sea level slope η_y in the northern CCS, with decreasing sea level to the north (a poleward surface pressure gradient) during the summer upwelling season. Assuming this pressure gradient is barotropic, we may anticipate onshore geostrophic flow throughout the water column. In the case of a steady and sufficiently large-scale mean APG acting alone, this onshore flux would need to be returned offshore at depth (balanced by bottom friction) to satisfy the coastal constraint and 2D mass balance (Thompson 1987). Although we cannot accurately determine the role of bottom stress, it is possible that the late-season near-bottom flow observed in Fig. 5 is a result of a mean APG.

To address whether a seasonal-mean APG existed in 2005, monthly averaged adjusted sea level from tide gauges all along the U.S. West Coast is plotted in Fig. 8. All records have annual-mean values removed to account for the unknown absolute sensor depths. Following Hickey and Pola (1983) we then added the long-term climatological mean [Fig. 8a; estimated relative to the 500-dbar level from Reid and Mantyla (1976)] before finally computing the monthly averages (Figs. 8b–m). Note that the 500-dbar level was the only reference deemed "well established" by Reid and Mantyla (1976), although they provided no error estimates; interannual variability remains unaccounted for with the Reid and Mantyla (1976) values. We estimated monthly values of η_y using least squares fits to six stations between La Push, WA, and Humboldt Bay, CA (gray lines and text in Fig. 8). Neah Bay, WA, was omitted because it consistently appeared anomalously high during the summer upwelling season in multiple years, which may result from surface Ekman accumulation of water near that site (see Fig. 4 of Tinis et al. 2006). Similarly, we omitted values from Astoria, OR, since they were consistently high in early summer (coincident with the Columbia River freshet) and often low later in the season in multiple years. Upwelling-only estimates of η_y, calculated during the same time periods considered in Fig. 5, are also included in Fig. 8 for the months of June–September (black text in the upper right of those panels). The monthly averages and upwelling-only means differ, but not enough to reverse the sign of η_y. From Fig. 8 it is evident that the description provided by Hickey and Pola (1983) holds true for 2005, with mean adjusted sea level decreasing poleward in July, August, and September. Our 2005 magnitudes for η_y are, however, larger by roughly an order of magnitude compared to those estimated using only the Neah Bay, WA, and Crescent City, CA, sites by Hickey and Pola (1983).

Given estimates of η_y at the coast from Fig. 8, we can estimate the hypothesized onshore/offshore mean geostrophic flow:

$$fu_G = -\rho_0^{-1} P_y = -g\eta_y . \tag{5}$$

For the upwelling-only means, if we assume offshore exponential decay of P_y (Werner and Hickey 1983; Brown et al. 1987; Chapman 1987) by a factor of $e^{-0.5} \approx 0.6$ to the

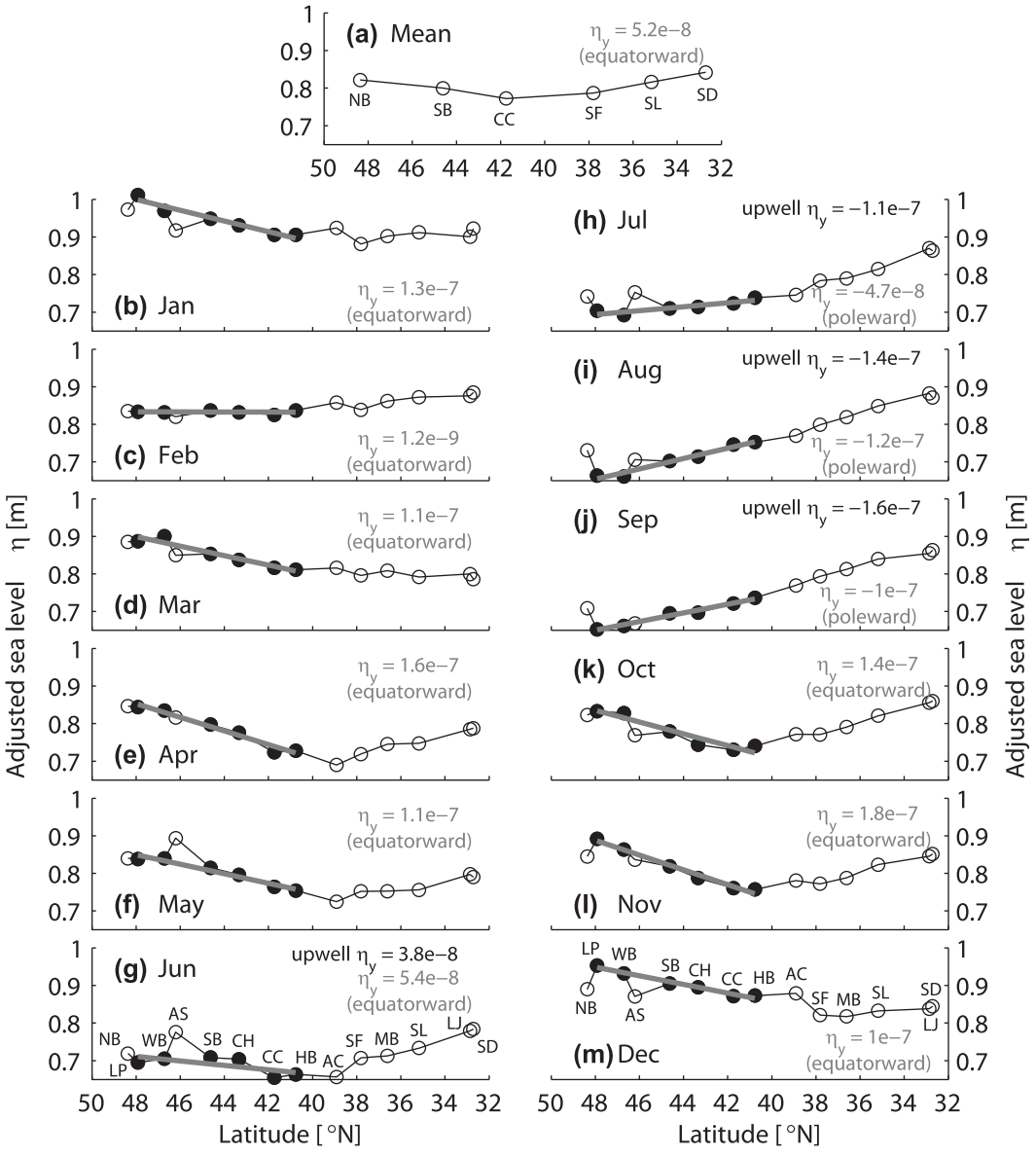

FIG. 8. (a) Long-term mean adjusted sea level (relative to the 500-dbar level) at select stations off the U.S. West Coast from Reid and Mantyla (1976). The value for Crescent City, CA, was taken from Hickey and Pola (1983). For reference, the value of the mean surface slope between Neah Bay, WA, and Newport, OR, is included in the gray text. (b)–(m) The 2005 monthly-mean adjusted sea level at 14 tide gauges along the U.S. West Coast from Neah Bay, WA, to San Diego, CA. Values at each station in (b)–(m) have the annual mean removed but include the long-term mean from panel (a) linearly interpolated to each site. Abbreviations for station names are given in panels (a), (g), and (m) and are Neah Bay (NB), La Push (LP), Willapa Bay (WB), Astoria (AS), South Beach (SB; Newport, OR), Charleston (CH), Crescent City (CC), Humboldt Bay (HB), Arena Cove (AC), San Francisco (SF), Monterey Bay (MB), Port San Luis (SL), La Jolla (LJ), and San Diego (SD). A linear regression using six stations between La Push, WA, and Humboldt Bay, CA, is also drawn [(b)–(m); gray line fitted to the black-filled circles] and provides an estimate of the monthly-mean alongshelf surface pressure gradient at the coast (gray text). As discussed in the text, stations at Neah Bay, WA, and Astoria, OR, were omitted from the regressions. Regression values using the same six stations, but for the upwelling-only time periods considered in Fig. 5, are displayed in the black text in panels (g)–(j). In the northern CCS, the long-term mean alongshelf surface pressure gradient in (a) is equatorward (Reid and Mantyla 1976) and reduces, but does not reverse, the magnitude of the summer 2005 poleward surface pressure gradient.

midshelf, we find that u_G is reasonably small: approximately $-0.2\,\mathrm{cm\,s^{-1}}$ offshore in June, $0.6\,\mathrm{cm\,s^{-1}}$ onshore in July, $0.8\,\mathrm{cm\,s^{-1}}$ onshore in August, and $0.9\,\mathrm{cm\,s^{-1}}$ onshore in September. These estimates (and the implied transports) may be compared to the surface layer–averaged Ekman velocities of 2.9, 4.1, 2.5, and $2.7\,\mathrm{cm\,s^{-1}}$ for the same months, respectively (section 5a). Given the multiple forcing agents in the coastal ocean, it is not immediately obvious how this remotely forced onshore/offshore mass flux should be balanced; the local wind stress is inadequate (Hickey and Pola 1983). For the northern CCS, the mean η_y extends over at least 700 km (and over a much greater distance during the summer upwelling months; Fig. 8), satisfying Thompson's (1987) large-scale criteria. If we assume mass balance does require u_G to be returned onshore or offshore in a compensating layer at depth, the sign of the "geostrophic return" u_{GR} would match that of the observed late-season mean near-bottom flow (Fig. 5).

It is striking that the seasonal change in vertical structure of the cross-shelf flow is coincident with the change in mean η_y from weak and equatorward in June to strong and poleward in August and September (cf. Figs. 2e and 5 with Fig. 8). Are the relative magnitudes of the late-season, near-bottom flows consistent with the simplest case of a 2D-balanced u_G? To estimate gross magnitudes for the hypothesized u_{GR}, a rough estimate of the thickness of the near-bottom layer (from the bottom to the first zero crossing of u_{proj} above the bottom in August and September; Fig. 5) is ~20 m. Assuming constant u_G over the upper water column is balanced by offshore transport in the bottom 20 m, the resulting estimates of u_{GR} for the months of July, August, and September are offshore at 1.5, 2.0, and $2.3\,\mathrm{cm\,s^{-1}}$, respectively. The order of magnitude is correct, but the values are 1–$1.5\,\mathrm{cm\,s^{-1}}$ too large.

Some fraction of the mean APG likely balances local wind stress. Ratios of the upwelling mean wind stress to the surface pressure gradient were 62%, 35%, and 28% in magnitude for July–September, respectively. Assuming these fractions describe the extent of the balance, the above u_{GR} estimates would reduce to within the 0.6–$1.7\,\mathrm{cm\,s^{-1}}$ range, in better agreement with the observations. However, this scenario also implies poleward alongshelf flow closer to the bottom than we observed. Regardless, it does appear plausible that a mean alongshelf sea level gradient could account for the late-season reversal to offshore near-bottom flow in Fig. 5.

3) The contribution from a large-scale mean alongshelf density gradient

Connolly et al. (2014) used numerical simulations to argue that a large-scale along-isobath density gradient is important over the northern CCS continental slope, forcing the California Undercurrent poleward. However, the extent to which an alongshelf density gradient ρ_y is important on the shelf is unknown. To estimate the mean alongshelf density gradient that would be required to overcome η_y and produce (geostrophically) the observed late-season near-bottom flow in Fig. 5, we again assume steady, linear, inviscid dynamics and rewrite (5) to include the density gradient term:

$$fu_G = -\rho_0^{-1}P_y = -g\eta_y - g\int_z^0 \rho_0^{-1}\rho_y\,dz'. \qquad (6)$$

Assuming exponential offshore decay of η_y as before, the late-season baroclinic pressure gradient would need to be $O(-2\times10^{-6})\,\mathrm{m\,s^{-2}}$, with average water column density increasing poleward. However, the historical mean summertime water property sections of Landry et al. (1989) suggest the depth-integrated density gradient is roughly one-third of that required and opposite in sign (depth-averaged density off WA is slightly less than off the coast of OR).

To make a more quantitative estimate, we considered all available midshelf ($50\,\mathrm{m} \le z_{\mathrm{bot}} \le 100\,\mathrm{m}$) CTD profiles collected within the latitude band 42°–48°N during July–September of multiple years (1972–2012). Data were taken from the RISE and ECOHAB-PNW cruises, the 2013 version of the World Ocean Database, and other recent and historical CTD collections. In total, only 588 profiles satisfied the above restrictions. Following Lentz (2008), each profile was interpolated to a 5-m vertical grid, and linear trends were fit to the data at each depth level. The resulting summertime-mean, depth-averaged (from 75-m depth to the surface), alongshelf density gradient was $\rho_y = -1.0\times10^{-6}\,(\mathrm{kg\,m^{-3}})\,\mathrm{m^{-1}}$, equivalent to an $O(7.4\times10^{-7})\,\mathrm{m\,s^{-2}}$ acceleration in (6) and in agreement with the estimate from Landry et al. (1989). The density gradient was poleward at the surface and decreased in magnitude with depth; below 50 m the trends were not significantly different from zero at 95% confidence limits. It remains unknown how representative this multiyear average is for any given year, but the August 2005 subset of data also indicated that the midshelf water column off WA was slightly less dense than off the coast of OR. Although ρ_y may impact vertical shear in the cross-shelf circulation, since the required alongshelf density gradient is opposite that suggested by the historical and more recent data, at present we must discount it as an explanation for the observed late-season near-bottom flow.

e. Seasonal relaxation from upwelling

As mentioned, the 2005 alongshelf wind stress decayed in magnitude (by ~33% for the monthly

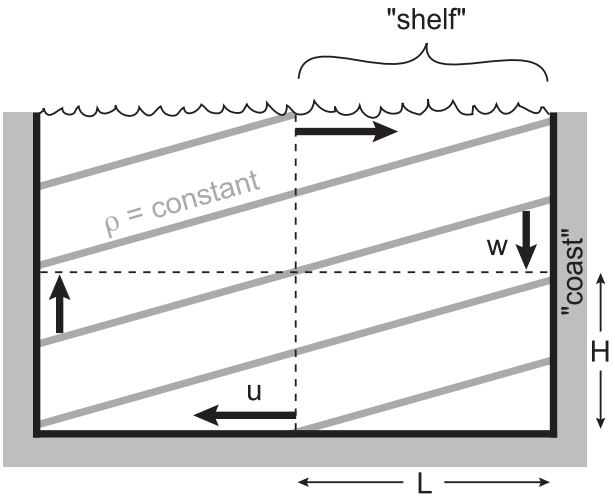

FIG. 9. Schematic section of isopycnals (ρ = constant) upwelled across a flat-bottom channel of half-width L and half-depth H. The isopycnals are allowed to fall toward a flat rest state with a vertical fall rate near the coast of w; the accompanying near-bottom cross-channel velocity is u. The right half of the channel approximates a shelf: isopycnals will fall to their respective levels at the channel midpoint, a distance L from the coast, similar to shelf isopycnals retreating to an offshore level in the coastal ocean.

upwelling averages) after mid-July and before the onset of storms at the end of September (Fig. 2a). Under decreasing surface stress it seems reasonable that upwelled isopycnals may migrate back down the shelf toward an eventual flat state. On the other hand, a downwelling-favorable, mean APG-forced, cross-shelf circulation could also lead to isopycnal "slumping." Assuming thermal wind dynamics apply at midshelf (e.g., Huyer et al. 1978; Strub et al. 1987), the late-season decrease in vertical shear of the alongshelf flow is consistent with a seasonal relaxation of isopycnals (Figs. 5c,e,g). Is the decreasing vertical shear also consistent with subsurface features of the u_{proj} profiles?

To address this question, consider an idealized, flat-bottom, frictionless channel in the absence of wind stress, but with isopycnals that slope up with constant value toward the "coast" (Fig. 9). The channel has half-width L and half-depth H. Assuming a 2D setting, if we imagine the isopycnals falling down toward a flat state (vertical arrows in Fig. 9), then mass conservation can be used to relate the vertical slumping rate w to the near-bottom (or near surface) cross-channel velocity u:

$$w = \frac{H}{L}u. \tag{7}$$

The right half of the idealized channel is analogous to a flat-bottom shelf where isopycnals may retreat to some offshore level, a distance L from the coast in Fig. 9. Near the coastal wall, the time rate of change of density is related to vertical advection of the background stratification:

$$\rho_t + w\rho_z = 0. \tag{8}$$

Substituting (7) into (8) and differentiating in the cross-channel direction results in

$$\rho_{xt} = -\frac{H}{L^2}u\rho_z, \tag{9}$$

where we have used $\partial_x \sim L^{-1}$. If we further use

$$N^2 = -\frac{g}{\rho_0}\rho_z, \tag{10}$$

with g gravitational acceleration, along with the thermal wind relation

$$v_z = -\frac{g}{\rho_0 f}\rho_x, \tag{11}$$

we can rewrite (9) as an equation for u in terms of the buoyancy frequency and the time variation of the alongshelf vertical shear v_z, quantities that may be readily evaluated from the mean N^2 profiles in Fig. 6 and the RN velocity record:

$$v_{zt} = -\frac{H}{L^2}\frac{N^2}{f}u. \tag{12}$$

A time series of vertically averaged interior (15–51-m depth) v_z from RN is plotted in Fig. 10. We estimated average trends for August and September in two ways: 1) linear fits to the data within each individual month (black dashed lines in Fig. 10), and 2) an exponential fit to the data spanning both months (thick gray line in Fig. 10). Using the mean slopes for each month, half-depth and shelf-width values of H = 100 m and L = 40 km, along with the interior mean N^2 values from Fig. 6, in (12) gives predicted near-bottom offshore u values of 1.4 cm s^{-1} in August and 0.3–0.6 cm s^{-1} in September, compared to observed values of 0.7 and 1.4 cm s^{-1} for the same months, respectively (Fig. 5). The exponential fit averaged over August and September (with a 2-month mean interior N^2) yields an offshore near-bottom u of 1.1 cm s^{-1}, which matches the 2-month average from the observations. Although the predictions for individual months are somewhat high or low in comparison to the near-bottom u_{proj} values in Figs. 5f and 5h, the overall agreement from the above simplified model suggests that a seasonal slumping of isopycnals could lead to the observed late-season near-bottom flow.

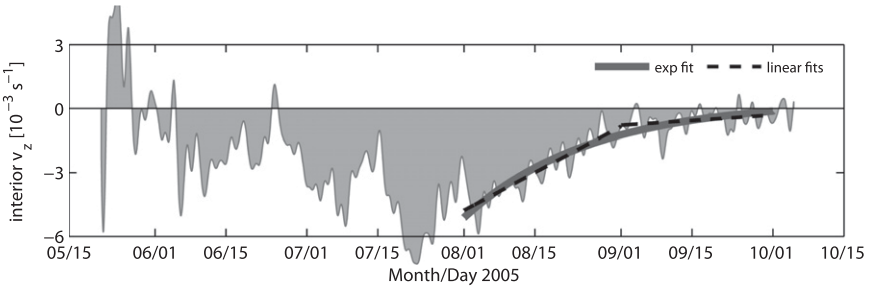

FIG. 10. Time series of the vertically averaged interior (15–51-m depth) alongshelf vertical shear v_z (shaded gray) from the RN velocity record showing a marked decrease after July. An exponential fit to v_z in the period spanning both August and September (thick gray line) and linear fits to v_z during individual months of August and September (dashed black lines) are also included.

6. Discussion

a. Mean APG or decaying surface wind stress?

As discussed above, two potentially related mechanisms could be responsible for the observed changes in the lower water column cross-shelf circulation: 1) a relatively abrupt switch in the mean APG from weak and equatorward in June to strong and poleward in August and September, and 2) a seasonal relaxation of upwelled isopycnals (inferred from decreasing v_z). The latter could itself be forced by the poleward mean APG or could possibly be related to the seasonal decay of local wind stress. However, because the mean APG becomes strongly poleward at around the same time that local winds begin to decay, it is unclear which leads to the decreasing v_z and the accompanying subsurface cross-shelf circulation (section 5d).

To help distinguish between these mechanisms, a multiyear record of monthly averaged interior v_z from another midshelf mooring in the region (the NH10 mooring off Newport, OR) is presented in Fig. 11c along with monthly estimates of τ^y (Fig. 11a) and η_y (Fig. 11b; computed as in Fig. 8). In general, interior v_z (averaged over 20–60-m depth) peaks and begins decreasing in magnitude prior to the summer minimum in τ^y. The only exceptions were 2000, which had variable v_z, and 2003, when the minimum shear and minimum surface stress happened to coincide. However, comparison of interior v_z with η_y shows that summertime changes in shear tend to track changes in the surface slope. When η_y reaches a negative value (a poleward pressure gradient), or in two cases a weakly positive value, there is a coincident decrease in the interior v_z. Interannual variability of the mean sea level slope that is unaccounted for with the Reid and Mantyla (1976) long-term estimate could help explain why v_z begins decreasing at times of weakly equatorward η_y in 2002 and 2004. If the Reid and Mantyla (1976) value is removed from η_y in Fig. 11b (the new zero line would fall at the top of the gray band), better agreement is found between η_y and v_z in 2002 and 2004. To help clarify the annual pattern, we also include averages of each parameter from 2000 to 2004 (Figs. 11e–h). From the 5-yr averages it is clear that v_z (Fig. 11g) decreases when η_y becomes poleward (Fig. 11f) despite the increasing mean equatorward τ^y (Fig. 11e). Although the decaying wind stress and increasing numbers of poleward alongshelf flow reversals undoubtedly contribute to upwelling relaxation as the season continues toward the fall transition, the data in Fig. 11 suggest that it is *initially* the mean APG, and not processes related to the decaying mean surface stress, that begins extracting energy from the flow by forcing upwelled isopycnals toward a flat state. From the relaxation model in section 5d, we infer a subsurface downwelling-favorable cross-shelf circulation during times of decreasing v_z that could lead to persistent offshore near-bottom flows.

b. Near-bottom temperature

To lend additional support to the observed mean u_{proj} structure in Fig. 5, we plot monthly averaged temperature from a near-bottom sensor on the RN mooring (at 65-m depth or 7 mab) in Fig. 11d. A downwelling-favorable circulation or relaxation of upwelled isopycnals should warm shelf bottom water. Monthly-mean temperature at RN decreased until August and then began a warming trend in September that continued to the end of the record in October. Although temperature is not definitive since a single downwelling wind stress event or a poleward alongshelf flow reversal could offset the record to a warmer state (our assumption is that the monthly averages smooth out such irregularities), the timing of the minimum temperature and the subsequent warming of the near-bottom shelf water is consistent with the arrival of mean offshore-directed near-bottom flows captured by u_{proj} in August and September (Fig. 5). Examination of the multiyear NH10 near-bottom

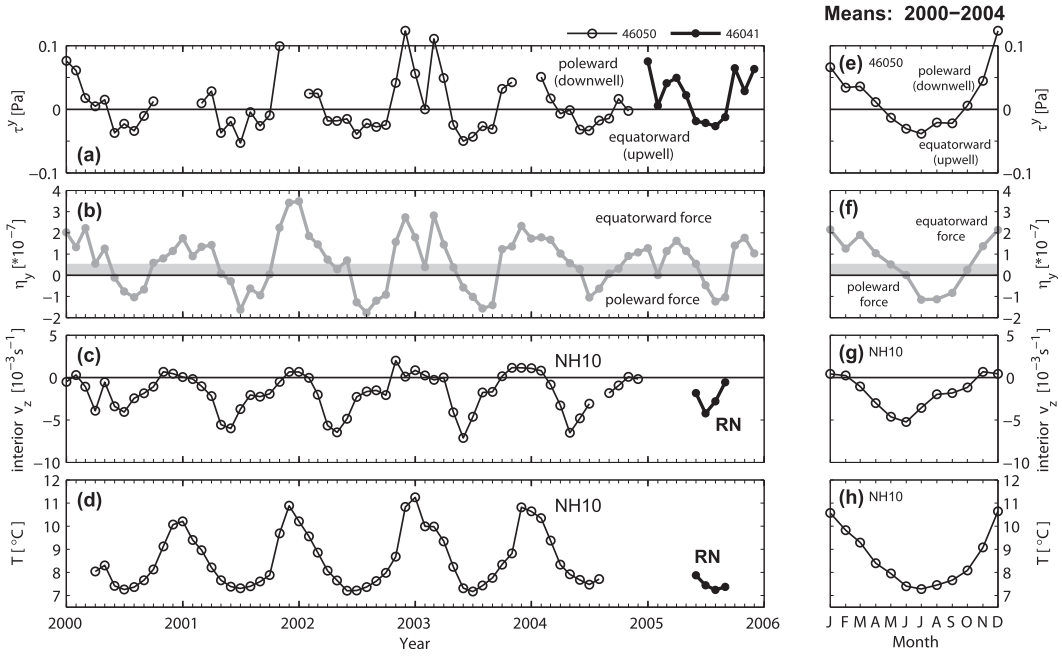

FIG. 11. (a) Monthly averaged alongshelf wind stress (positive poleward, downwelling favorable) at two different stations: NDBC buoy 46041 off Cape Elizabeth, WA (thick line with filled circles in 2005), and buoy 46050 off Newport, OR (thin line with open circles from 2000 to 2004). (b) Monthly averaged estimates of the mean alongshelf sea level slope in the northern CCS (positive poleward or an equatorward force) calculated from linear regressions to data from the tide gauges between La Push, WA, and Humboldt Bay, CA (as in Fig. 8). The horizontal gray band extends vertically from zero to the value of the regional long-term mean from Reid and Mantyla (1976), which is included in the sea level slope estimates. (c) Monthly estimates of the vertically averaged interior alongshelf vertical shear from the RN mooring off WA (thick dotted line), and the GLOBEC NH10 mooring off Newport, OR (81-m bottom depth; thin line with open circles). (d) Monthly averaged near-bottom temperature estimates from the RN (thick dotted line) and NH10 moorings (thin line with open circles). In each of (a)–(d), the *x* axis tick marks appear at the start of each month, with the larger marks denoting 1 Jan of each year. To aid in pattern interpretation, (e)–(h) display averages of the 2000–04 data from (a) to (d).

temperature record (sensor at 71-m depth or 10 mab; Fig. 11d) indicates that the minimum temperature at that site similarly occurs after the regional transition to a poleward η_y (Fig. 11b) and the peak in interior v_z (Fig. 11c). This suggests that near-bottom flows similar to Fig. 5 may be a common late-season occurrence in the northern CCS.

c. *Effect of the late-season near-bottom flow on the overlying cross-shelf velocity profile*

Although the poleward mean APG appears to flatten upwelled isopycnals and give rise to the mean near-bottom offshore flow observed late in the upwelling season, so far we have not accounted for the observed seasonal enhancement of the interior return flow; any APG-forced geostrophic cross-shelf flow should be reasonably uniform with depth in the interior (ignoring the poorly constrained ρ_y contribution). Our suggestion is that the presence of the near-bottom offshore flow requires the offshore surface Ekman transport to be compensated by onshore flux within the interior. Evidence supporting this is provided in Fig. 12. At the RN site, u_{proj} near the surface is well correlated with τ^y (r = 0.69 at zero lag for June–September; Fig. 12a), consistent with Ekman dynamics. The u_{proj} record 30 m deeper, within the interior return flow layer, shows a markedly different pattern (Fig. 12b). Early in the season, interior u_{proj} and τ^y are poorly correlated ($r = -0.3$ for June–July). However, by approximately late July or early August u_{proj} at 33-m depth is strongly anticorrelated with τ^y ($r = -0.6$ for August–September), and this is true for other interior depths as well (not shown). The timing of the change from little correlation to significant anticorrelation occurs after the mean APG has become poleward (Fig. 8) and corresponds to the development of the offshore near-bottom u_{proj} layer in Figs. 5f and 5h. Thus, although the enhanced interior return flow compensates surface wind forcing, its existence appears to be a consequence of the persistent APG-forced near-bottom flow.

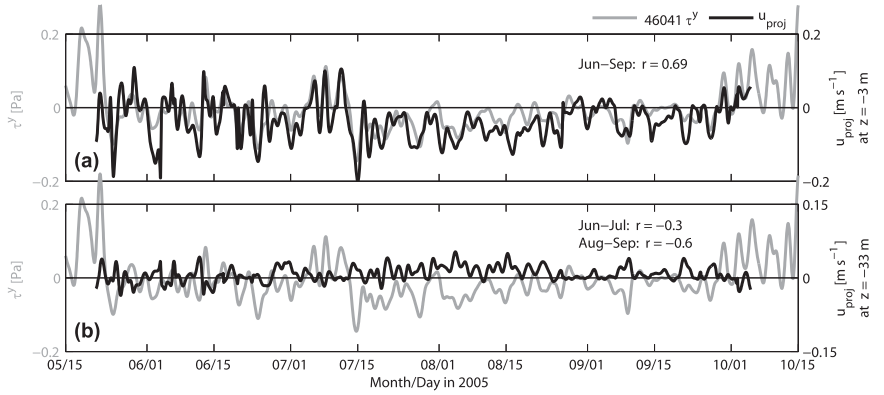

FIG. 12. Comparisons of the record of alongshelf surface wind stress (gray lines) from NDBC buoy 46041with observed u_{proj} (black lines) at (a) 3-m depth and (b) within the interior at 33-m depth. Zero-lag correlation coefficients spanning June–September in (a), and 2-month-long early and late-season periods in (b) are labeled in the upper right of both panels. Note that the u_{proj} velocity scale changes from (a) to (b).

7. Conclusions and summary

This study used observations to investigate the seasonally changing structure of cross-shelf circulation at a midshelf location in the northern CCS. The analysis was made possible by development of a new method that allows isolation of a 2D-balanced estimate of the subtidal cross-shelf circulation from a highly variable flow field. The technique projects the stream-normal flow onto the cross-shelf coordinate in order to remove meander- or eddy-induced biases from the observed circulation. Comparison of the resulting cross-shelf circulation with estimates made using another commonly applied technique highlighted the biases inherent in the standard approach and revealed a previously unrealized, seasonally changing vertical structure.

Early in the season (June), the upwelling-mean offshore surface transport was compensated by weak onshore flow throughout the lower water column. In July, a mean onshore return flow developed within the water column interior. This return flow strengthened (by more than a factor of 2) and shoaled throughout the remainder of the upwelling season. At the same time, a mean offshore-directed near-bottom flow developed, and strengthened, while vertical shear in the alongshelf flow decayed. The resulting upwelling-mean cross-shelf circulation profile during the latter half of the upwelling season was three layered to within 9 m of the bottom; offshore flow existed in the surface 10–15 m, an onshore return flow existed within the interior (spanning depths of approximately 15–45 m), and a third offshore-directed layer existed at depth. Near-bottom temperature observations documented a late-season warming, consistent with offshore flow in the near-bottom layer. The timing of the development and strengthening of both the interior return flow and the near-bottom layer were consistent with the seasonally changing direction and magnitude of the large-scale alongshelf sea level gradient and a relaxation of upwelled isopycnals.

Our interpretation of the observed late-season, upwelling-favorable, cross-shelf circulation over the midshelf is summarized in a schematic cartoon (Fig. 13). Under an equatorward alongshelf wind stress, surface Ekman transport is directed offshore (Fig. 13a). Propagating CTWs induce a small ($\leq 1\,\mathrm{cm\,s^{-1}}$) and nearly vertically uniform interior cross-shelf flow that may be directed on- or offshore depending on the phase of the passing wave (Fig. 13b). However, in this study the September mean CTW-induced cross-shelf flow was near zero. Flows within 9 mab were not observed, so it remains unknown what role bottom stress plays in forcing the near-bottom cross-shelf flow (Fig. 13c). The large-scale poleward mean APG forces a weak cross-shelf flow that is directed onshore throughout the interior water column (Fig. 13d). If other forces such as the wind stress are of insufficient magnitude to balance the mean APG, then the onshore transport should be returned offshore at depth (Fig. 13d), implying balance through bottom friction. The existence of the near-bottom layer with offshore-directed transport, in turn, requires the offshore surface Ekman transport to occur within the interior (Fig. 13a) to satisfy 2D coastal mass balance. It is primarily the wind stress and the poleward mean APG that give rise to the observed late-season profile that is composed of the surface Ekman layer, the enhanced interior onshore return flow, and the offshore-directed near-bottom flow (Fig. 13e).

Implications of the seasonally changing vertical structure are wide ranging. Shallow onshore return flows may deliver nutrient-depleted waters to the surface relative to

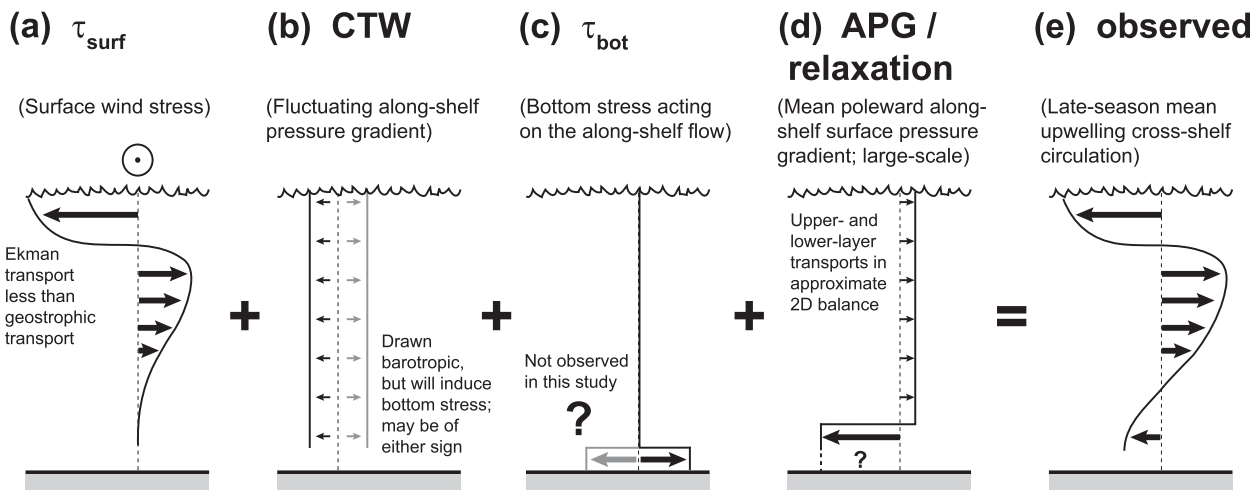

FIG. 13. Schematic diagram representing one interpretation of the late-season, mean, upwelling-favorable, cross-shelf circulation. Flows directed to the left/right are offshore/onshore. (a) Offshore surface Ekman transport resulting from an upwelling-favorable alongshelf wind stress, and a compensating onshore interior transport. (b) The interior cross-shelf circulation profile resulting from a passing first-mode CTW. The CTW transport may be of either sign depending on the phase of the passing wave. In the present study, this contribution to the cross-shelf velocity had a near-zero mean. (c) Bottom stress was not observed in this study, but may lead to onshore or offshore transport depending on the sign of the alongshelf flow. (d) The cross-shelf circulation profile resulting from a large-scale poleward mean alongshelf surface pressure gradient. If other forces such as the alongshelf wind stress are of insufficient magnitude to balance the pressure gradient, the onshore transport should be returned offshore in a near-bottom layer (implying balance by bottom friction). This circulation profile is also consistent with a relaxation of upwelled isopycnals. The lower portion of the offshore layer in (d) was not observed in this study, as indicated by the small question mark and dashed connection to the bottom. The presence of the offshore near-bottom layer in (d) requires surface Ekman transport to be compensated in the interior, as drawn in (a), to satisfy coastal mass balance. (e) The observed mean cross-shelf circulation during late-season upwelling-favorable conditions.

deeper return flows, suggesting potential seasonal changes in biological productivity or community structure. Late-season, offshore-directed, near-bottom flows may similarly lead to seasonality in shelf water property budgets. At present, additional data are required to test statistical relationships between near-bottom cross-shelf flows, water properties, wind stress, and alongshelf pressure gradients. A comprehensive description of the dynamics is not possible without a more complete dataset. Future observational studies should make every effort to capture as much of the boundary layers as possible. Because the large-scale mean APG appears to play an important role in the vertical structure of cross-shelf circulation, advances in remote sensing of the alongshelf and cross-shelf coastal pressure distributions are needed to address the larger shelfwide response.

Acknowledgments. This work originated as part of the Pacific Northwest Toxins (PNWTOX) project and was supported by grants from the Coastal Ocean Program of the National Oceanic and Atmospheric Administration (NOAA; NA09NOS4780180) and the National Science Foundation (NSF; OCE-0942675 and OCE-1332753). The statements, findings, conclusions, and recommendations are those of the authors and do not reflect the views of NSF, NOAA, or the Department of Commerce. Tide gauge data used in this paper were obtained from the National Ocean Service of NOAA and the Joint Archive for Sea Level project, a cooperative effort between the U.S. National Oceanographic Data Center and the University of Hawaii Sea Level Center. U.S. GLOBEC NH10 data used in Fig. 11 were made available by P. M. Kosro. We thank N. B. Kachel for processing CTD data and S. L. Geier for discussions on ADCP processing. Comments from two anonymous reviewers helped to improve this manuscript.

REFERENCES

Allen, J. S., and P. K. Kundu, 1978: On the momentum, vorticity and mass balance on the Oregon shelf. *J. Phys. Oceanogr.,* **8,** 13–27, doi:10.1175/1520-0485(1978)008<0013:OTMVAM>2.0.CO;2.

——, and R. L. Smith, 1981: On the dynamics of wind-driven shelf currents. *Philos. Trans. Roy. Soc. London,* **A302,** 617–634, doi:10.1098/rsta.1981.0187.

Austin, J. A., and J. A. Barth, 2002: Variation in the position of the upwelling front on the Oregon shelf. *J. Geophys. Res.,* **107,** 3180, doi:10.1029/2001JC000858.

Battisti, D. S., and B. M. Hickey, 1984: Application of remote wind-forced coastal trapped wave theory to the Oregon and Washington coasts. *J. Phys. Oceanogr.,* **14,** 887–903, doi:10.1175/1520-0485(1984)014<0887:AORWFC>2.0.CO;2.

Beardsley, R. C., R. Limeburner, and L. K. Rosenfeld, 1985: CODE-2 moored array and large-scale data report. Woods Hole Oceanographic Institution Tech. Rep. WHOI-85-35, 234 pp.

Blanton, J., E. Wenner, F. Werner, and D. Knott, 1995: Effects of wind-generated coastal currents on the transport of blue crab megalopae on a shallow continental shelf. *Bull. Mar. Sci.,* **57,** 739–752. [Available online at http://www.ingentaconnect.com/content/umrsmas/bullmar/1995/00000057/00000003/art00017?crawler=true.]

Brink, K. H., D. Halpern, and R. L. Smith, 1980: Circulation in the Peruvian upwelling system near 15°S. *J. Geophys. Res.,* **85,** 4036–4048, doi:10.1029/JC085iC07p04036.

Brown, W. S., J. D. Irish, and C. D. Winant, 1987: A description of subtidal pressure field observations on the northern California continental shelf during the Coastal Ocean Dynamics Experiment. *J. Geophys. Res.,* **92,** 1605–1635, doi:10.1029/JC092iC02p01605.

Bryden, H. L., 1978: Mean upwelling velocities on the Oregon continental shelf during summer 1973. *Estuarine Coastal Mar. Sci.,* **7,** 311–327, doi:10.1016/0302-3524(78)90085-3.

Chapman, D. C., 1987: Application of wind-forced, long, coastal-trapped wave theory along the California coast. *J. Geophys. Res.,* **92,** 1798–1816, doi:10.1029/JC092iC02p01798.

Connolly, T. P., B. M. Hickey, I. Shulman, and R. E. Thomson, 2014: Coastal trapped waves, alongshore pressure gradients, and the California Undercurrent. *J. Phys. Oceanogr.,* **44,** 319–342, doi:10.1175/JPO-D-13-095.1.

Csanady, G. T., 1978: The arrested topographic wave. *J. Phys. Oceanogr.,* **8,** 47–62, doi:10.1175/1520-0485(1978)008<0047:TATW>2.0.CO;2.

Dever, E. P., 1997a: Subtidal velocity correlation scales on the northern California shelf. *J. Geophys. Res.,* **102,** 8555–8571, doi:10.1029/96JC03451.

——, 1997b: Wind-forced cross-shelf circulation on the northern California shelf. *J. Phys. Oceanogr.,* **27,** 1566–1580, doi:10.1175/1520-0485(1997)027<1566:WFCSCO>2.0.CO;2.

——, and S. J. Lentz, 1994: Heat and salt balances over the northern California shelf in winter and spring. *J. Geophys. Res.,* **99,** 16 001–16 017, doi:10.1029/94JC01228.

——, C. E. Dorman, and J. L. Largier, 2006: Surface boundary-layer variability off northern California, USA, during upwelling. *Deep-Sea Res. II,* **53,** 2887–2905, doi:10.1016/j.dsr2.2006.09.001.

Farrell, T. M., D. Bracher, and J. Roughgarden, 1991: Cross-shelf transport causes recruitment to intertidal populations in central California. *Limnol. Oceanogr.,* **36,** 279–288, doi:10.4319/lo.1991.36.2.0279.

Federiuk, J., and J. S. Allen, 1995: Upwelling circulation on the Oregon continental shelf. Part II: Simulations and comparisons with observations. *J. Phys. Oceanogr.,* **25,** 1867–1889, doi:10.1175/1520-0485(1995)025<1867:UCOTOC>2.0.CO;2.

Freeland, H. J., W. R. Crawford, and R. E. Thomson, 1984: Currents along the Pacific coast of Canada. *Atmos.–Ocean,* **22,** 151–172, doi:10.1080/07055900.1984.9649191.

Gan, J., and J. S. Allen, 2002: A modeling study of shelf circulation off northern California in the region of the Coastal Ocean Dynamics Experiment: Response to relaxation of upwelling winds. *J. Geophys. Res.,* **107,** 3123, doi:10.1029/2000JC000768.

Geyer, W. R., 1993: Three-dimensional tidal flow around headlands. *J. Geophys. Res.,* **98,** 955–966, doi:10.1029/92JC02270.

Gill, A. E., 1982: *Atmosphere–Ocean Dynamics.* Academic Press, 662 pp.

Hamilton, P., and M. Rattray Jr., 1978: A numerical model of the depth-dependent, wind-driven upwelling circulation on a continental shelf. *J. Phys. Oceanogr.,* **8,** 437–457, doi:10.1175/1520-0485(1978)008<0437:ANMOTD>2.0.CO;2.

Hickey, B. M., 1984: The fluctuating longshore pressure gradient on the Pacific Northwest shelf: A dynamical analysis. *J. Phys. Oceanogr.,* **14,** 276–293, doi:10.1175/1520-0485(1984)014<0276:TFLPGO>2.0.CO;2.

——, 1989: Patterns and processes of circulation over the Washington continental shelf and slope. *Coastal Oceanography of Washington and Oregon,* M. R. Elsevier Oceanography Series, Vol. 47, Elsevier, 41–115.

——, and N. E. Pola, 1983: The seasonal alongshore pressure gradient on the west coast of the United States. *J. Geophys. Res.,* **88,** 7623–7633, doi:10.1029/JC088iC12p07623.

——, and Coauthors, 2010: River influences on shelf ecosystems: Introduction and synthesis. *J. Geophys. Res.,* **115,** C00B17, doi:10.1029/2009JC005452.

Huyer, A., R. D. Pillsbury, and R. L. Smith, 1975: Seasonal variation of the alongshore velocity field over the continental shelf off Oregon. *Limnol. Oceanogr.,* **20,** 90–95, doi:10.4319/lo.1975.20.1.0090.

——, R. L. Smith, and E. J. C. Sobey, 1978: Seasonal differences in low-frequency current fluctuations over the Oregon continental shelf. *J. Geophys. Res.,* **83,** 5077–5089, doi:10.1029/JC083iC10p05077.

——, ——, and T. Paluszkiewicz, 1987: Coastal upwelling off Peru during normal and El Niño times, 1981–1984. *J. Geophys. Res.,* **92,** 14 297–14 307, doi:10.1029/JC092iC13p14297.

Jacox, M. G., and C. A. Edwards, 2011: Effects of stratification and shelf slope on nutrient supply in coastal upwelling regions. *J. Geophys. Res.,* **116,** C03019, doi:10.1029/2010JC006547.

Johnson, D. F., L. W. Botsford, R. D. Methot Jr., and T. C. Wainwright, 1986: Wind stress and cycles in Dungeness crab (*Cancer magister*) catch off California, Oregon, and Washington. *Can. J. Fish. Aquat. Sci.,* **43,** 838–845, doi:10.1139/f86-103.

Kalkwijk, J. P. T., and R. Booij, 1986: Adaptation of secondary flow in nearly-horizontal flow. *J. Hydraul. Eng.,* **24,** 19–37, doi:10.1080/00221688609499330.

Kosro, P. M., 1987: Structure of the coastal current field off northern California during the Coastal Ocean Dynamics Experiment. *J. Geophys. Res.,* **92,** 1637–1654, doi:10.1029/JC092iC02p01637.

——, W. T. Peterson, B. M. Hickey, R. K. Shearman, and S. D. Pierce, 2006: Physical versus biological spring transition: 2005. *Geophys. Res. Lett.,* **33,** L22S03, doi:10.1029/2006GL027072.

Kundu, P. K., and J. S. Allen, 1976: Some three-dimensional characteristics of low-frequency current fluctuations near the Oregon coast. *J. Phys. Oceanogr.,* **6,** 181–199, doi:10.1175/1520-0485(1976)006<0181:STDCOL>2.0.CO;2.

——, ——, and R. L. Smith, 1975: Modal decomposition of the velocity field near the Oregon coast. *J. Phys. Oceanogr.,* **5,** 683–704, doi:10.1175/1520-0485(1975)005<0683:MDOTVF>2.0.CO;2.

Landry, M. R., J. R. Postel, W. K. Peterson, and J. Newman, 1989: Broad-scale distributional patterns of hydrographic variables on the Washington/Oregon shelf. *Coastal Oceanography of Washington and Oregon,* Elsevier Oceanographic Series, Vol. 47, Elsevier, 1–40.

Large, W. G., and S. Pond, 1981: Open ocean momentum flux measurements in moderate to strong winds. *J. Phys. Oceanogr.,* **11,** 324–336, doi:10.1175/1520-0485(1981)011<0324:OOMFMI>2.0.CO;2.

Lentz, S. J., 1987: A heat budget for the northern California shelf during CODE 2. *J. Geophys. Res.,* **92,** 14 491–14 509, doi:10.1029/JC092iC13p14491.

——, 1992: The surface boundary layer in coastal upwelling regions. *J. Phys. Oceanogr.,* **22,** 1517–1539, doi:10.1175/1520-0485(1992)022<1517:TSBLIC>2.0.CO;2.

——, 2001: The influence of stratification on the wind-driven cross-shelf circulation over the North Carolina shelf. *J. Phys. Oceanogr.,* **31,** 2749–2760, doi:10.1175/1520-0485(2001)031<2749:TIOSOT>2.0.CO;2.

——, 2008: Observations and a model of the mean circulation over the Middle Atlantic Bight continental shelf. *J. Phys. Oceanogr.,* **38,** 1203–1221, doi:10.1175/2007JPO3768.1.

——, and J. H. Trowbridge, 1991: The bottom boundary layer over the northern California shelf. *J. Phys. Oceanogr.,* **21,** 1186–1201, doi:10.1175/1520-0485(1991)021<1186:TBBLOT>2.0.CO;2.

——, and D. C. Chapman, 2004: The importance of nonlinear cross-shelf momentum flux during wind-driven coastal upwelling. *J. Phys. Oceanogr.,* **34,** 2444–2457, doi:10.1175/JPO2644.1.

MacFadyen, A., B. M. Hickey, and M. G. G. Foreman, 2005: Transport of surface waters from the Juan de Fuca eddy region to the Washington coast. *Cont. Shelf Res.,* **25,** 2008–2021, doi:10.1016/j.csr.2005.07.005.

——, ——, and W. P. Cochlan, 2008: Influences of the Juan de Fuca Eddy on circulation, nutrients, and phytoplankton production in the northern California Current System. *J. Geophys. Res.,* **113,** C08008, doi:10.1029/2007JC004412.

Marchesiello, P., and P. Estrade, 2010: Upwelling limitation by onshore geostrophic flow. *J. Mar. Res.,* **68,** 37–62, doi:10.1357/002224010793079004.

——, J. Lefevre, A. Vega, X. Couvelard, and C. Menkes, 2010: Coastal upwelling, circulation and heat balance around New Caledonia's barrier reef. *Mar. Pollut. Bull.,* **61,** 432–448, doi:10.1016/j.marpolbul.2010.06.043.

Melton, C., L. Washburn, and C. Gotschalk, 2009: Wind relaxations and poleward flow events in a coastal upwelling system on the central California coast. *J. Geophys. Res.,* **114,** C11016, doi:10.1029/2009JC005397.

Pollard, R., 1973: Interpretation of near-surface current meter observations. *Deep-Sea Res. Oceanogr. Abstr.,* **20,** 261–268, doi:10.1016/0011-7471(73)90015-6.

Pringle, J. M., and E. P. Dever, 2009: Dynamics of wind-driven upwelling and relaxation between Monterey Bay and Point Arena: Local-, regional-, and gyre-scale controls. *J. Geophys. Res.,* **114,** C07003, doi:10.1029/2008JC005016.

Rabalais, N. N., R. E. Turner, and W. J. Wiseman Jr., 2002: Gulf of Mexico hypoxia, A.K.A. "the dead zone." *Annu. Rev. Ecol. Syst.,* **33,** 235–263, doi:10.1146/annurev.ecolsys.33.010802.150513.

Ramp, S. R., J. D. Paduan, I. Shulman, J. Kindle, F. L. Bahr, and F. Chavez, 2005: Observations of upwelling and relaxation events in the northern Monterey Bay during August 2000. *J. Geophys. Res.,* **110,** C07013, doi:10.1029/2004JC002538.

Reid, J. L., and A. W. Mantyla, 1976: The effect of the geostrophic flow upon coastal sea elevations in the northern North Pacific Ocean. *J. Geophys. Res.,* **81,** 3100–3110, doi:10.1029/JC081i018p03100.

Relvas, P., and E. D. Barton, 2002: Mesoscale patterns in the Cape Sao Vicente (Iberian Peninsula) upwelling region. *J. Geophys. Res.,* **107,** 3164, doi:10.1029/2000JC000456.

——, and ——, 2005: A separated jet and coastal counterflow during upwelling relaxation off Cape Sao Vicente (Iberian Peninsula). *Cont. Shelf Res.,* **25,** 29–49, doi:10.1016/j.csr.2004.09.006.

Rossi, V., M. Feng, C. Pattiaratchi, M. Roughan, and A. M. Waite, 2013: On the factors influencing the development of sporadic upwelling in the Leeuwin Current system. *J. Geophys. Res. Oceans,* **118,** 3608–3621, doi:10.1002/jgrc.20242.

Roughgarden, J., S. Gaines, and H. Possingham, 1988: Recruitment dynamics in complex life cycles. *Science,* **241,** 1460–1466, doi:10.1126/science.11538249.

Rozovskii, I. L., 1957: *Flow of Water in Bends of Open Channels* (translated from Russian). Academy of Sciences of the Ukrainian SSR, 233 pp.

Rudnick, D. L., and R. E. Davis, 1988: Mass and heat budgets on the northern California continental shelf. *J. Geophys. Res.,* **93,** 14 013–14 024, doi:10.1029/JC093iC11p14013.

Send, U., R. C. Beardsley, and C. D. Winant, 1987: Relaxation from upwelling in the Coastal Ocean Dynamics Experiment. *J. Geophys. Res.,* **92,** 1683–1698, doi:10.1029/JC092iC02p01683.

Smith, R. L., 1978: Poleward propagating perturbations in currents and sea levels along the Peru coast. *J. Geophys. Res.,* **83,** 6083–6092, doi:10.1029/JC083iC12p06083.

——, 1981: A comparison of the structure and variability of the flow field in three coastal upwelling regions: Oregon, northwest Africa, and Peru. *Coastal Upwelling,* F. A. Richards, Ed., Amer. Geophys. Union, 107–118, doi:10.1029/CO001p0107.

——, A. Huyer, J. S. Godfrey, and J. A. Church, 1991: The Leeuwin Current off Western Australia, 1986–1987. *J. Phys. Oceanogr.,* **21,** 323–345, doi:10.1175/1520-0485(1991)021<0323:TLCOWA>2.0.CO;2.

Stommel, H., and A. Leetmaa, 1972: Circulation on the continental shelf. *Proc. Natl. Acad. Sci. USA,* **69,** 3380–3384, doi:10.1073/pnas.69.11.3380.

Strub, P. T., J. S. Allen, A. Huyer, R. L. Smith, and R. C. Beardsley, 1987: Seasonal cycles of currents, temperatures, winds, and sea level over the northeast Pacific continental shelf: 35°N to 48°N. *J. Geophys. Res.,* **92,** 1507–1526, doi:10.1029/JC092iC02p01507.

Thompson, R. O. R. Y., 1987: Continental-shelf-scale model of the Leeuwin Current. *J. Mar. Res.,* **45,** 813–827, doi:10.1357/002224087788327190.

Tinis, S. W., R. E. Thomson, C. F. Mass, and B. M. Hickey, 2006: Comparison of MM5 and meteorological buoy winds from British Columbia to northern California. *Atmos.–Ocean,* **44,** 65–81, doi:10.3137/ao.440105.

Weingartner, T. J., S. L. Danielson, and T. C. Royer, 2005: Freshwater variability and predictability in the Alaska Coastal Current. *Deep-Sea Res. II,* **52,** 169–191, doi:10.1016/j.dsr2.2004.09.030.

Werner, F. E., and B. M. Hickey, 1983: The role of a longshore pressure gradient in Pacific Northwest coastal dynamics. *J. Phys. Oceanogr.,* **13,** 395–410, doi:10.1175/1520-0485(1983)013<0395:TROALP>2.0.CO;2.

Winant, C. D., R. C. Beardsley, and R. E. Davis, 1987: Moored wind, temperature, and current observations made during coastal ocean dynamics experiments 1 and 2 over the northern California shelf and upper slope. *J. Geophys. Res.,* **92,** 1569–1604, doi:10.1029/JC092iC02p01569.

Wing, S. R., J. L. Largier, L. W. Botsford, and J. F. Quinn, 1995: Settlement and transport of benthic invertebrates in an intermittent upwelling region. *Limnol. Oceanogr.,* **40,** 316–329, doi:10.4319/lo.1995.40.2.0316.

Wiseman, W. J., N. N. Rabalais, R. E. Turner, S. P. Dinnel, and A. MacNaughton, 1997: Seasonal and interannual variability within the Louisiana coastal current: Stratification and hypoxia. *J. Mar. Syst.,* **12,** 237–248, doi:10.1016/S0924-7963(96)00100-5.

Zamudio, L., and M. Lopez, 1994: On the effect of the alongshore pressure gradient on numerical simulations over the northern California continental shelf. *J. Geophys. Res.,* **99,** 16 117–16 129, doi:10.1029/94JC01116.